Journal of Atmospheric and Solar-Terrestrial Physics 92 (2013) 43–50

Contents lists available at SciVerse ScienceDirect

Journal of Atmospheric and Solar-Terrestrial Physics

journal homepage: www.elsevier.com/locate/jastp

Statistical characteristics of high frequency gravity waves observed by OH airglow imaging from Tirunelveli (8.7°N)

V. Lakshmi Narayanan *, S. Gurubaran

Equatorial Geophysical Research Laboratory, Indian Institute of Geomagnetism, Tirunelveli-627011, India

A R T I C L E I N F O

Article history:
Received 24 March 2012
Received in revised form
4 September 2012
Accepted 4 September 2012
Available online 12 September 2012

Keywords:
Quasi-monochromatic gravity waves
High frequency gravity waves
OH airglow imaging

A B S T R A C T

The importance of high frequency gravity waves in the upper mesospheric region is now well recognized. In this study, we examine the characteristics of high frequency gravity waves observed in OH emission by an all-sky airglow imager operated from Tirunelveli (8.7°N, 77.8°E) during 2007. Background wind information was obtained from co-located MF radar from which the intrinsic wave parameters were estimated. The study reveals predominance of meridionally propagating waves. The phase speeds of the waves were found to be relatively higher during equinoxes compared to solstices. Nearly half of the observed waves showed vertically evanescent behavior. We probed the relative importance of various terms in the gravity wave dispersion relation. We found that the contribution from the wind shear and curvature terms are not significant for statistical studies of high frequency wave events. Nevertheless, they may be important for case studies of individual wave events. Moreover, the analysis revealed the importance of wave reflections arising out of oppositely directed background winds for the short horizontal wavelength gravity waves. This could explain the observed predominance in the propagation towards the meridional directions.

© 2012 Elsevier Ltd. All rights reserved.

1. Introduction

Atmospheric gravity waves propagating from the lower atmosphere attain large amplitudes and play dominant role in the energetics and dynamics of the mesosphere region. It is expected that high frequency gravity waves with periods less than an hour carry upward a large momentum flux and energy density (Fritts and Vincent, 1987; Vincent, 1987). All-sky airglow imaging technique provides unique datasets to study such high frequency gravity waves. The images capture two dimensional horizontal structures of high frequency gravity waves that perturb the airglow emissions. Several studies in the past were carried out from different locations to study the characteristics of these high frequency waves (Ejiri et al., 2003; Li et al., 2011; Medeiros et al., 2007; Nakamura et al., 1999; Nielsen et al., 2009; Pautet et al., 2005; Suzuki et al., 2004, 2009a, 2009b; Taylor et al., 1997). However, still the global distribution of the high frequency gravity waves and their spatial variabilities remain unknown. Further, information regarding their source mechanisms and distribution of the source regions are intense topics of research.

In this study, we discuss the characteristics of high frequency gravity waves observed in OH emissions from Tirunelveli (8.7°N, 77.8°E) during different seasons of 2007. This is the first study on the statistical characteristics of high frequency gravity waves over Indian sector covering all the seasons. Earlier studies from Indian sector have focused on particular events or dataset covering few days in a particular season (Mukherjee, 2003, Narayanan et al., 2009a, 2009b, 2010, 2012b; Pragati et al., 2010). The observational site is located close to the southern tip of the peninsular India and is situated at mean sea level. As a result, the sky is often cloudy restricting the number of useful observations to 35 nights in the months of January, February, March, May, August and October 2007. The number of useful nights of observations and relevant information are provided in Table 1. We have categorized data from March and October months as corresponding to equinox conditions. No separation is made as spring and fall equinox due to availability of data for only one day during October. However, since the equinoxes correspond to the transition conditions between the solstices, we expect that the phase speed and wavelength distributions might be similar during both equinoxes. Any difference in their propagation directions need to be addressed in future study incorporating a larger dataset. In addition, it may be seen that more than half of the data was collected during winter periods owing to less convective activity. This is expected to induce a bias towards winter season in the overall estimates. However, as will be shown later, the distribution of wavelengths are similar in all the seasons. Further, we herein show and discuss the parameters obtained within each season separately.

* Corresponding author. Tel.: +91 462 2521465; fax: +91 462 2521466.
E-mail address: narayananvlwins@gmail.com (V. Lakshmi Narayanan).

1364-6826/$ - see front matter © 2012 Elsevier Ltd. All rights reserved.
http://dx.doi.org/10.1016/j.jastp.2012.09.002

In addition to the propagation characteristics, we utilize colocated MF radar wind measurements to study the intrinsic wave parameters and relative magnitudes of terms arising in the dispersion relation of gravity waves. The details of the instruments and data analysis method adopted herein are briefly explained in next section. Section 3 presents the results followed by summary and conclusions in Section 4. The results indicate the importance of wave reflection by means of oppositely directed background wind. This effect will not be significant for waves with horizontal wavelengths of ~50 km and above.

2. Instrumentation and data analysis

The frontend optics of the all-sky airglow imager comprises of a fisheye lens, shutter and a pair of achromats forming telecentric arrangement. A six position filter wheel follows the telecentric lens pair. One of the filters is a broadband filter covering the wavelength range of 705–928 nm with a notch at ~865 nm. This filter captures the near infrared emissions emanating from the OH radicals in the upper mesosphere region centered around 87 km. The notch at ~865 nm suppresses the O_2 band emissions emerging from a layer centered at ~94 km altitudes. The light coming out of the interference filters is reimaged into a CCD camera. The CCD is a back-illuminated one with 512×512 pixels. The light intensity falling on the pixels are digitized into 16 bits. The CCD is monochromatic and is not a deep depleted one. The camera system is thermoelectrically cooled to temperatures below -70 °C (dark charge is 0.0023 electrons/pixel/s at -70 °C) during data acquisition. Further information on the instrument can be found at Narayanan et al. (2009b). This instrument is already used to study the mesospheric and thermospheric airglow features (Narayanan et al., 2009a, 2012a).

The image acquisition procedure and data analysis method utilized in this work are similar to those described in Narayanan et al. (2012b). A group of OH images were acquired successively with an exposure time of 1 min (on rare occasions 2 min exposure was used) before acquiring images with other filters. The successive images within the group are subjected to time differencing (TD) method (Swenson and Mende, 1994). Thus the time difference between the images used in TD method is usually 1 min, which is always less than the buoyancy time period. The TD images are projected into equidistance grid and the wave parameters, namely, horizontal wavelength, apparent phase velocity and propagation direction, are extracted manually, without subjecting them to spectral analysis. The maximum percentage errors in the estimations of horizontal wavelengths and apparent phase velocities are within 10% and 20%, respectively. The propagation azimuth is measured within an accuracy of $\pm 2°$. By selecting several wave events randomly, we verified that the parameters extracted by TD method is consistent with that obtained by full image processing methods discussed in Garcia et al. (1997) and Narayanan et al. (2009b). Fig. 1 shows examples of wave events obtained during different seasons of 2007.

We utilize the co-located MF radar wind observations to estimate background winds and intrinsic wave parameters. The operating frequency of the radar is 1.98 MHz and the winds are derived by means of spaced antenna technique at every 2 km altitude range between 68 km and 98 km. However, the true vertical resolution of the radar is ~4 km. Further details of the MF radar system can be obtained from Rajaram and Gurubaran (1998) and the references cited therein. The average winds between 84 and 90 km altitudes over every 20 min interval are evaluated to overcome gaps in radar data. The propagation azimuths of the waves are taken note of and the winds are calculated along those azimuths. The background winds were obtained from averages of these 20 min wind data for the duration over which the waves were observed. In addition to the background winds, we also estimate wind shears between 84 and 90 km altitudes. Wind curvatures (second derivatives of horizontal wind with height) are not considered due to large uncertainties in their estimations arising out of data gaps in radar winds. For the gravity waves propagating opposite to the background mean flow, the values of the calculated background winds will be given as negative numbers.

It may be noticed that not all wave-like fluctuations observed in all-sky airglow images are quasi-monochromatic (QM) gravity waves. Instability features called ripples and prominent mesospheric frontal systems were also observed along with QM gravity waves (Narayanan et al., 2009b, 2012b). The frontal systems are rare events while the ripples are relatively frequent. The instabilities responsible for generation of ripples arise due to the extreme wind shears or superadiabatic lapse rates occurring in thin regions (typically less than 2–3 km in thickness) in the upper mesosphere. If the instabilities are due to extreme wind shears, they are called dynamical instabilities and if they arise out of superadiabatic lapse rates, they are known as convective instabilities.

Several of earlier workers starting from Nakamura et al. (1999) have assumed that all wave-like features with horizontal wavelengths less than ~17 km are ripples (e.g., Suzuki et al., 2011). However, it is not correct to discriminate waves and

Table 1
Observation details and number of events during different seasons.

Season	Months	Number of nights	Number of useful hours	Number of events	Number of waves/h
Winter	Jan & Feb	15	66	104	1.58
Summer	May & Aug	9	31	45	1.45
Equinox	Mar & Oct	11	32	61	1.91
Total	–	35	129	210	1.63

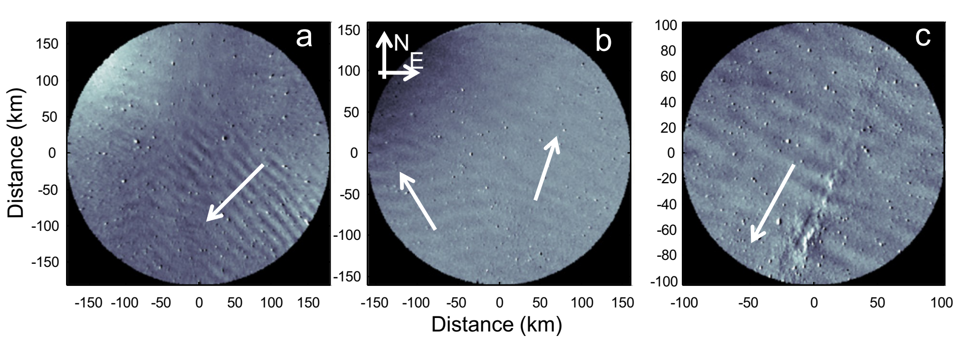

Fig. 1. Sample images showing gravity wave events during different seasons. (a) 04:44 IST on 25 January, 2007; (b) 19:53 IST on 19 March, 2007; and (c) 02:33 IST on 21 May, 2007. The x and y axis show distance in km. The arrows represent the propagation direction of the wave events.

ripples only based on their wavelengths, as many QM waves with smaller wavelengths might get wrongly identified as ripples. Especially, as will be shown in the next section, the horizontal wavelength distribution for waves observed over Tirunelveli peaks near 17 km. Since ripples are instability features, they are expected to drift along with the background mean flow. Hence, their intrinsic phase speeds are expected to be few m/s. We adopt the following criteria to identify the ripples: (i) Wave-like features with wavelengths less than 9 km were considered as ripples. This criterion is based on our observations that most of the events with wavelengths less than 9 km appeared patchy and at times they advected in the directions that are not perpendicular to their phase fronts; (ii) All events that displayed intrinsic phase speeds less than 15 m/s and wavelengths less than 17 km are considered as ripples. It may be noted that this criterion is essentially dependent on the smaller phase speeds expected for the ripple events. This criterion is expected to identify ripple events with wavelengths between 9 and 17 km; (iii) All events with wavelengths greater than 17 km are considered as gravity waves. After identifying the ripple events based on the above mentioned criteria and neglecting them, we are left with 210 QM wave events to study their statistical characteristics.

3. Results and discussion

The distributions of observed horizontal wavelengths are shown in Fig. 2((a)–(d)). It may be seen that most of the waves possessed wavelengths between 10 and 25 km in all the seasons. The average horizontal wavelength was 18.7 km. Comparisons with previous studies of statistical characteristics of such waves from different sites show that several sites have witnessed such shorter horizontal wavelengths (Ejiri et al., 2003; Medeiros et al., 2007; Nielsen et al., 2009; Pautet et al., 2005; Suzuki et al., 2004, 2009a, 2009b; Taylor et al., 1997). To our knowledge, only few reports were made for sites within 15° geographic latitudes and all of them were from the Southern Hemisphere (Medeiros et al., 2007; Nakamura et al., 2003; Suzuki et al., 2004, 2009b; Taylor et al., 1997).

Fig. 3((a)–(d)) shows the distribution of the apparent phase velocities. From the figure, it may be noticed that most of the waves had apparent phase speeds between 30 and 90 m/s. This is similar to the previous reports (Suzuki et al., 2009a, 2009b). The phase speeds of the waves observed during the equinox periods appear to be higher than those of the waves observed during solstices. The distribution of the intrinsic phase velocities is shown in Fig. 4((a)–(d)). The intrinsic phase velocities were also higher during equinoxes than those during solstices. In solstice periods the intrinsic phase velocities of most of the waves were less than 90 m/s.

The propagation directions of the waves are shown in Fig. 5((a)–(d)). The waves are separated into eight 45° bins centered over eight directions viz. the north, northeast, east, etc. 0° azimuth corresponds to the north and 90° azimuth to the east. The figure reveals anisotropic propagation of the waves. Highest anisotropy is found for summer season in which almost all of the waves propagated towards the south and southwest. Apart from this, the overall trend reveals predominant meridional propagation of the waves and minimum number of waves propagated in the zonal directions. The directionalities of the waves indicate possible source regions and effects of filtering due to middle atmospheric winds. A separate study is being undertaken regarding the probable sources of the waves and the effect of middle atmospheric winds on the observed waves. The results will be presented elsewhere separately.

The distributions of apparent and intrinsic wave periods are shown in Figs. 6 and 7((a)–(d)), respectively. The apparent wave periods typically lie below 13 min and the intrinsic wave periods lie below 18 min. Since we have excluded the ripple events, the waves with intrinsic wave periods less than buoyancy time period (~4.75 min) are supposedly evanescent ones.

The dispersion relationship for high frequency gravity waves neglecting the coriolis and acoustic compression effects is given

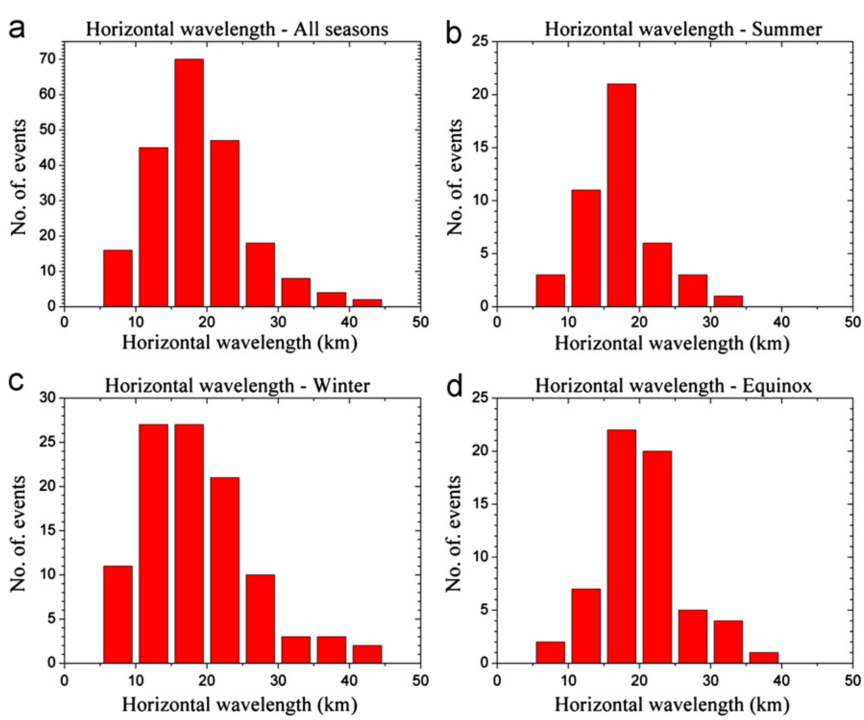

Fig. 2. Distribution of horizontal wavelengths: (a) all seasons, (b) summer, (c) winter and (d) equinoxes.

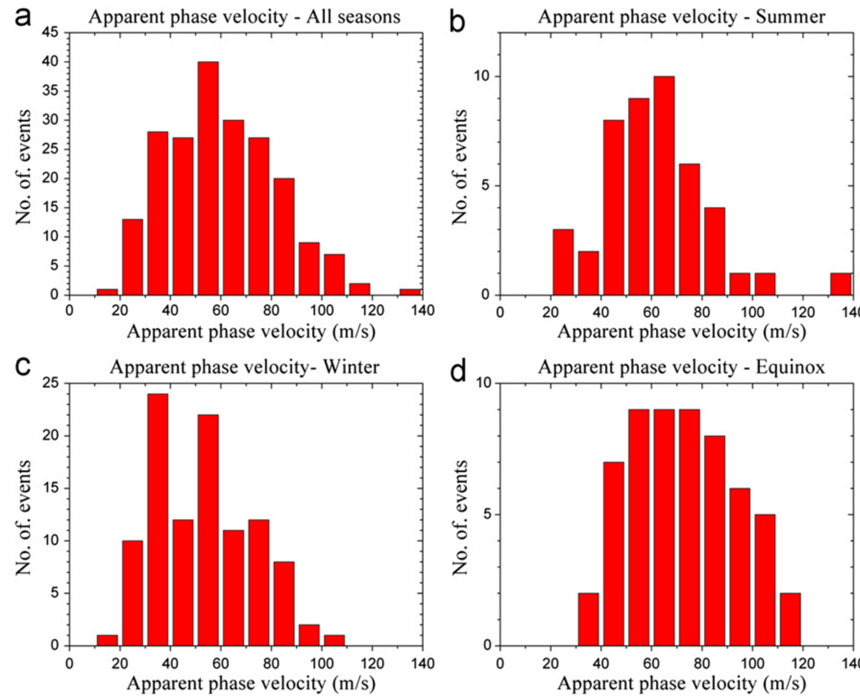

Fig. 3. Distribution of apparent phase velocities: (a) all seasons, (b) summer, (c) winter and (d) equinoxes.

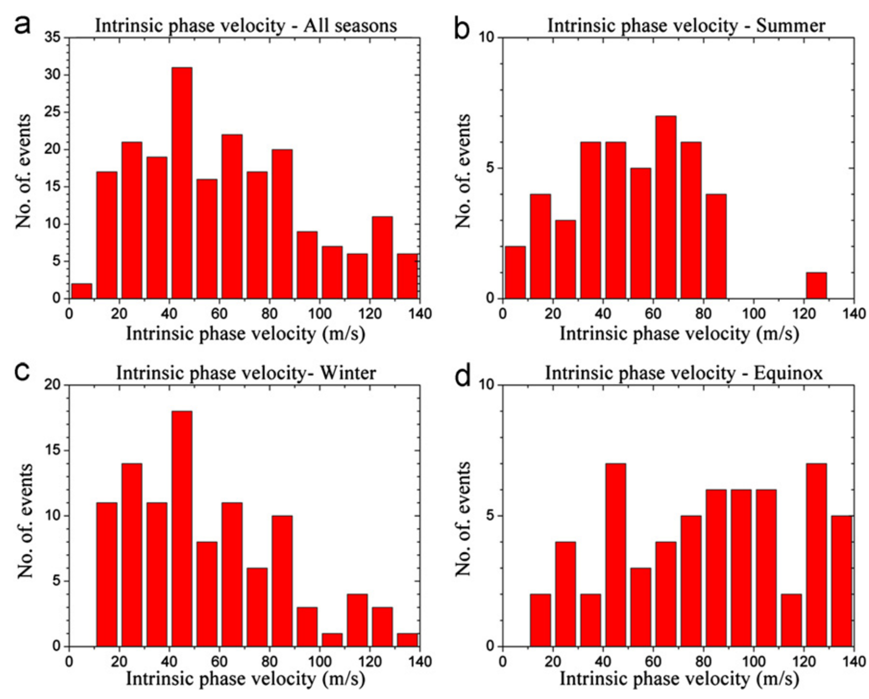

Fig. 4. Distribution of intrinsic phase velocities: (a) all seasons, (b) summer, (c) winter and (d) equinoxes.

by the following equation (Nappo, 2002).

$$m^2 = \frac{N^2}{(u-c)^2} - \frac{u_{zz}}{(u-c)} + \frac{1}{H}\frac{u_z}{(u-c)} - \frac{1}{4H^2} - k^2 \quad (1)$$

where, m and k are respectively the vertical and horizontal wave numbers, N is the buoyancy frequency, u and c are respectively the background wind and the apparent phase speed of the wave, u_z and u_{zz} are the first and second derivatives of background wind and H is the scale height. From the climatological mean temperatures obtained by SABER instrument between 2003 and 2009, we infer that the value of N is $\sim$0.022 rad/s around 85 km altitudes. We use this value in our calculations. The scale height is taken as 6 km.

Since we do not have estimations of wind curvatures, we excluded the second term in the above dispersion relation. We have also calculated the vertical wave numbers without considering the wind shear term (the third term). A comparison is made between m^2 values obtained with and without shear term. The comparison showed that the consideration of wind shear is not important for statistical studies. Out of the 210 wave events, for 14 events we did not have wind shear estimations due to data

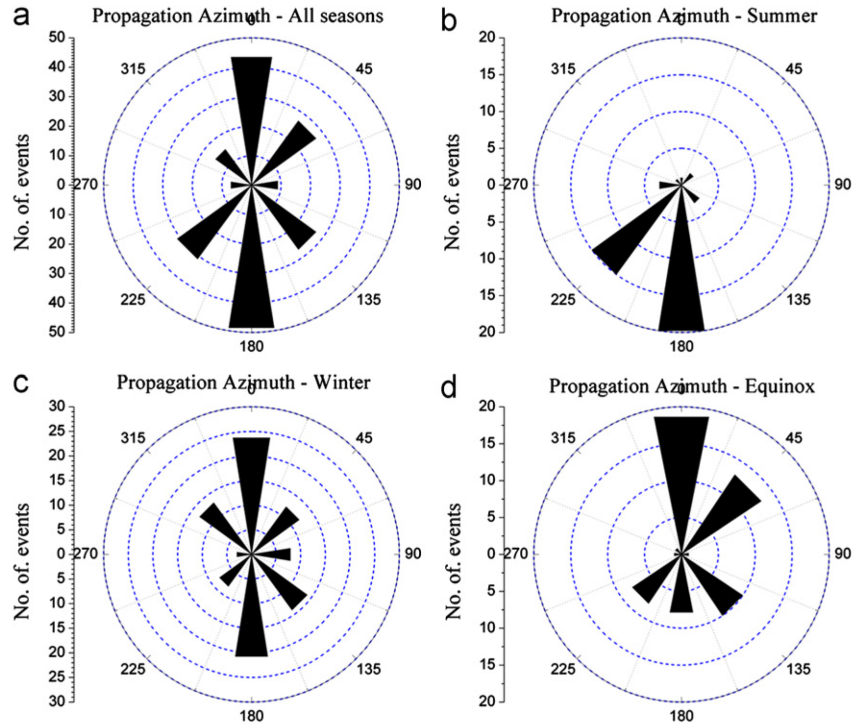

Fig. 5. Distribution of propagation direction of the waves: (a) all seasons, (b) summer, (c) winter and (d) equinoxes.

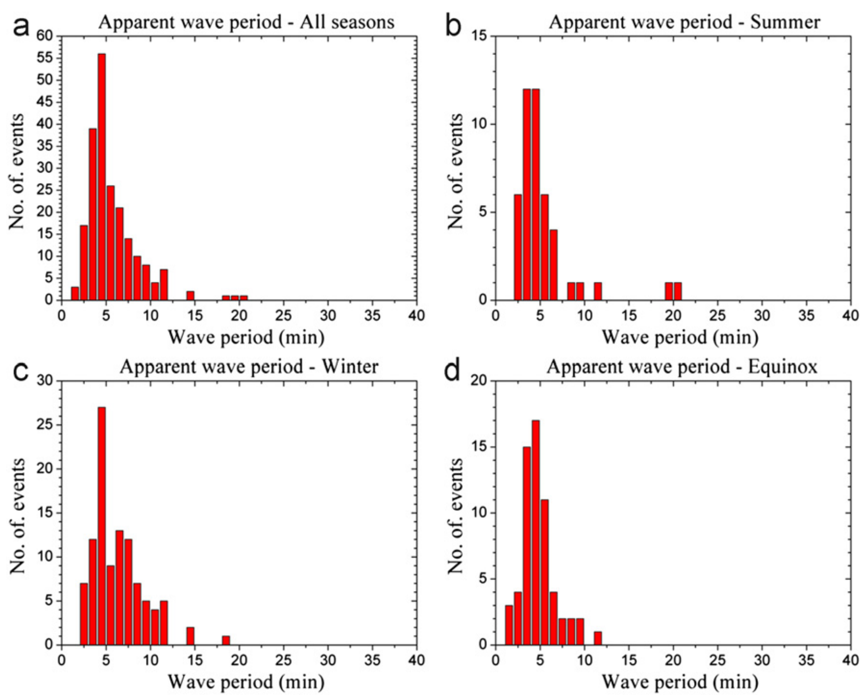

Fig. 6. Distribution of apparent wave periods: (a) all seasons, (b) summer, (c) winter and (d) equinoxes.

gaps in radar winds. In the remaining 196 events, it is found that the sign of m^2 remained same for 186 events in both the sets. Further, in both the sets, 97 events had m^2 values less than 0 indicating wave evanescence in OH emission altitudes. However, there are differences in the magnitude of m^2 values. This implies that incorporation of wind shears in individual case studies of the wave events may be important. The averages of vertical wavelengths estimated with and without shear term are 24.0 km and 26.6 km, respectively.

We have also estimated the relative importance of the four terms in the dispersion relation for high frequency gravity waves that are observed in imaging studies. The N^2 and k^2 terms are of comparable magnitudes and play important role in determining the propagation characteristics of a high frequency gravity wave. The magnitude of the k^2 term will decrease with increasing horizontal wavelengths. On the average, from our dataset, the contribution of wind shear term is estimated to be ~16% of N^2 term and that of the scale height term (fourth term in Eq (1)) is

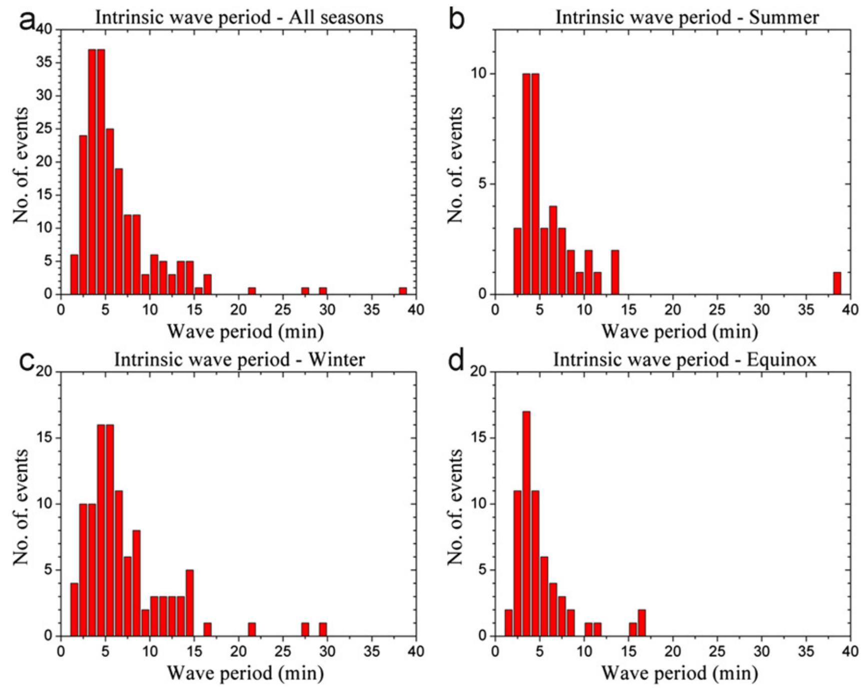

Fig. 7. Distribution of intrinsic wave periods: (a) all seasons, (b) summer, (c) winter and (d) equinoxes.

estimated to be $\sim$8% of N^2 term. Since the curvatures in wind will not occur frequently, the effect of curvature term is also expected to be considerably lesser than the N^2 and k^2 terms, except near critical levels and levels of reflections. At this juncture, we would like to point out that we have studied shears between 84 and 90 km. The contribution of shear term may be higher if shear data of finer resolutions are used. However, it is unlikely that the shear term may become dominant except near intense shear regions which might occur for short durations on restricted altitudinal range. Anyhow, in this study, for studying the vertical propagation characteristics of the gravity waves observed over Tirunelveli, we use the m^2 values calculated with shear term. Since we do not have wind shear estimations for 10 and 4 wave events respectively from summer and winter periods, their vertical propagation characteristics were not studied.

Our analysis shows that nearly half of the observed waves were vertically evanescent in nature (i.e. $m^2<0$, resulting in imaginary vertical wave number). Fig. 8 shows the percentages of evanescent and propagating waves in bar graph format. It may be noticed from the figure that the evanescent waves outnumbered the propagating waves during equinox periods while in the solstice periods the propagating waves were more in number. This is directly related to the observation of higher intrinsic phase speeds for the waves observed during the equinox periods (see Fig. 4). Since the horizontal wavelengths were similar (see Fig. 2) for all the seasons, the k^2 term in Eq. (1) would not vary considerably between the seasons. But during equinoxes, the higher intrinsic phase velocities result in a reduction in the N^2 term of the dispersion relation. As a result the m^2 becomes negative implying the evanescent nature of the waves.

Physical insight of the above explanation would be clear when the simple relationship between the background winds (u), apparent (c) and intrinsic phase velocities ($|u-c|$) is considered. The intrinsic phase velocities would be higher than the apparent phase velocities for the waves moving opposite to the background wind. In such cases, the wave frequencies are Doppler shifted to higher frequencies. The converse is true for the waves propagating in the direction of the background wind. Once if the wave intrinsic

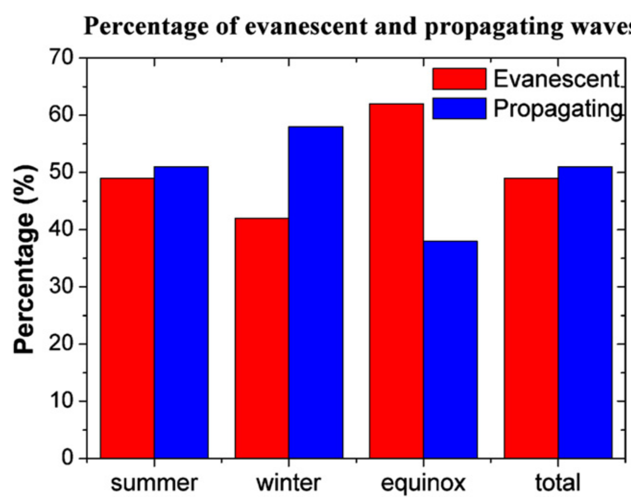

Fig. 8. Percentage of evanescent and propagating waves.

frequency approaches the buoyancy frequency, then the oscillations induced by the waves will become more and more vertical and the wave propagation direction would be more and more horizontal. Thus, the wave undergoes overturning and reflection.

About half of the observed events propagated opposite to the background wind as shown in Fig. 9. In order to study the role of oppositely directed background wind in generating wave evanescence, we have plotted the total number of evanescent waves observed during each season and the number of evanescent waves propagated opposite to the background wind. The plot is shown in Fig. 10. The figure clearly reveals that a majority of evanescent waves are propagating opposite to the background wind. The percentages of evanescent waves with oppositely directed background winds are 65%, 83% and 76% during summer, winter and equinox periods respectively. Totally 77% of the evanescent waves were propagating opposite to the background wind. This observation shows that the gravity waves with shorter

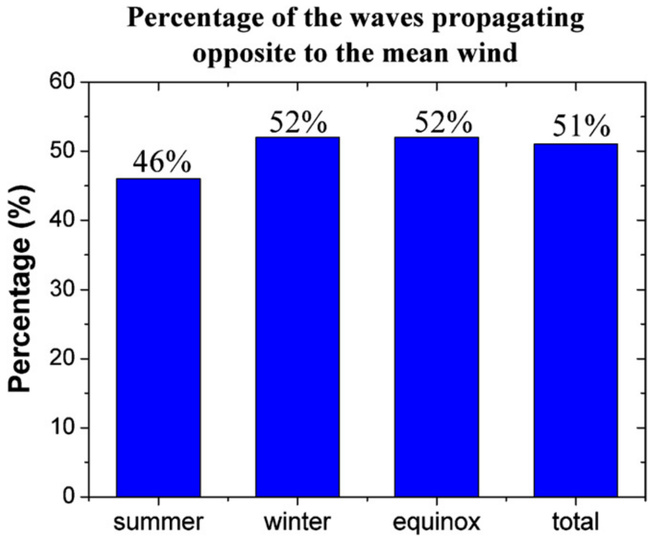

Fig. 9. Percentage of waves propagating opposite to the background wind.

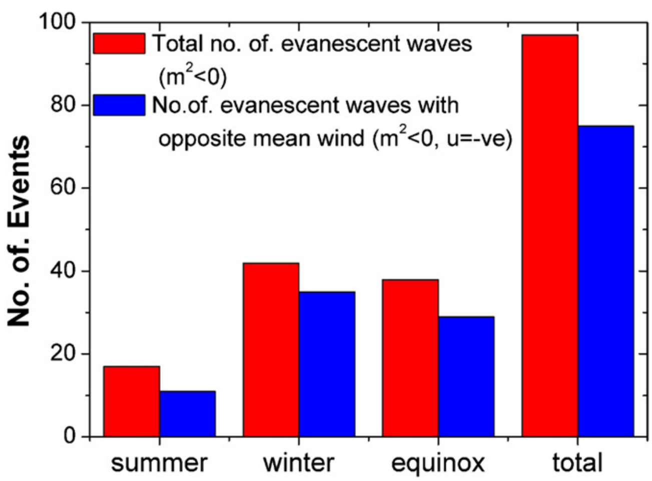

Fig. 10. The total number of evanescent waves and the number of evanescent waves with oppositely directed background wind.

horizontal wavelengths, typically below 50 km (i.e. those waves having larger value for k^2 term), may undergo reflection when they propagate opposite to mean background winds. A detailed case study of such a wave reflection is discussed by Narayanan et al. (2010).

For the waves propagating opposite to the background winds, vertical wavelengths will become higher due to Doppler shifting towards higher intrinsic frequencies (Li et al., 2011). Since airglow imagers are more sensitive to longer vertical wavelength waves, Li et al. (2011) suggested that there might be a bias towards observation of waves propagating against the mean background wind. If our observation of more number of evanescent waves propagating opposite to the background wind results from such a bias, it is supposed to be seen for freely propagating waves also. We plot the total number of freely propagating waves and the number of freely propagating waves with oppositely directed mean background wind in Fig. 11. The figure reveals that only a small portion of the freely propagating waves are moving opposite to the background mean wind. Therefore, observation of more number of evanescent waves propagating opposite to the background wind does not result from observational bias. The oppositely directed mean background winds do play an important role

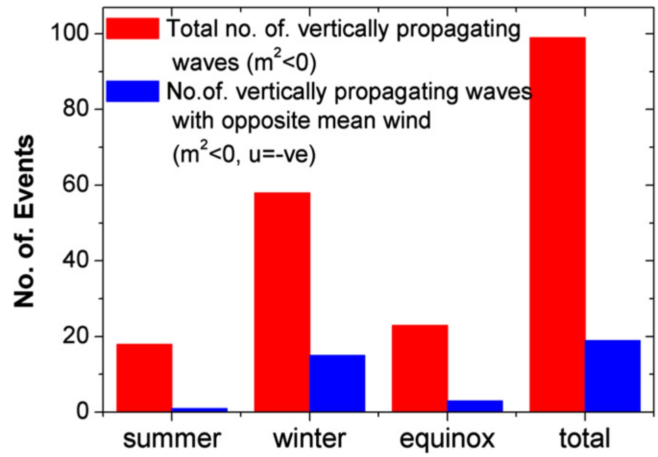

Fig. 11. The total number of freely propagating waves and the number of freely propagating waves with oppositely directed background wind.

in bringing about wave reflection and evanescence in the high frequency regime of atmospheric gravity waves.

Therefore, in addition to wave filtering by critical level absorption in the middle atmosphere, such reflections are also important for these high frequency gravity waves. This might be the reason for the observed predominance of meridional propagation of high frequency gravity waves during all the seasons. Such a predominant meridional propagation is also noticed in the previous studies (Ejiri et al., 2003; Suzuki et al., 2004; Walterscheid et al., 1999). It appears that in the middle atmosphere both critical level absorption and reflections due to oppositely directed background winds would have played a role in filtering out the waves in zonal directions. Since the background winds are weak in meridional directions, both the filtering mechanisms might not have significantly filtered the high frequency waves and allowed them to propagate to higher altitudes in the meridional directions. It may be noted that this type of wave reflection and associated filtering will not be significant for waves with larger horizontal wavelengths (typically above 50 km) due to the smaller value of k^2 term.

4. Summary and Conclusions

In this work, we have discussed the characteristics of high frequency gravity waves observed in OH airglow images over Indian sector covering all the seasons of 2007. However, about half of the events studied were acquired during winter months. To our knowledge, this is the first study of statistical characteristics of such waves from India covering all the seasons. The study revealed predominant meridional propagation of high frequency gravity waves in the upper mesosphere over Southern Peninsular India. The highest anisotropy was found during summer period in which almost all the waves were traveling towards the south and southwest. The wavelengths are similar in all the seasons and the distribution peaks at ~18 km. Both the apparent and intrinsic phase velocities were relatively higher during equinoxes than that during solstices.

The periodicities of observed waves are close to that of the buoyancy time period. Nearly half of the waves were found to be evanescent in nature, with more evanescent waves in equinox period than those in solstices. Further analysis with background wind information showed that many waves might have Doppler-shifted to higher frequencies by oppositely directed background winds and they became evanescent. This implies the importance of reflection by means of oppositely directed background winds for the high frequency gravity waves. Such reflections along with the critical level absorptions in the middle atmosphere might be responsible for filtering of the zonally propagating waves, thereby resulting in the observed predominance of meridional propagation in upper mesospheric altitudes. We have also studied the relative magnitudes of different terms in the dispersion relationship and found that the wind shear and scale height terms are not important for statistical studies, though they are supposedly important for individual case studies. The analyses of the waves are being extended with a larger dataset and the results will be presented later.

Acknowledgments

The lead author V.L.N. thanks the Director, Indian Institute of Geomagnetism for offering a research scholarship. This work is supported by the Department of Science and Technology, Government of India.

References

Ejiri, M.K., Shiokawa, K., Ogawa, T., Igarashi, K., Nakamura, T., Tsuda, T., 2003. Statistical study of short-period gravity waves in OH and OI nightglow images at two separated sites. Journal of Geophysical Research 108, 4679, http://dx.doi.org/10.1029/2002JD002795.

Fritts, D.C., Vincent, R.A., 1987. Mesospheric momentum flux studies at Adelaide, Australia: observations and a gravity wave-tidal interaction model. Journal of the Atmospheric Sciences 44, 605–619.

Garcia, F.J., Taylor, M.J., Kelley, M.C., 1997. Two-dimensional spectral analysis of mesospheric airglow image data. Applied Optics 36, 7374–7385.

Li, Z., Liu, A.Z., Lu, X., Swenson, G.R., Franke, S.J., 2011. Gravity wave characteristics from OH airglow imager over Maui. Journal of Geophysical Research 116, D22115, http://dx.doi.org/10.1029/2011JD015870.

Medeiros, A.F., Takahashi, H., Buriti, R.A., Fechine, J., Wrasse, C.M., Gobbi, D., 2007. MLT gravity wave climatology in the South America equatorial region observed by airglow imager. Annales Geophysicae 25, 399–406.

Mukherjee, G.K., 2003. The signature of short-period gravity waves imaged in the OI 557.7 nm and near infrared OH nightglow emissions over Panhala. Journal of Atmospheric and Solar-Terrestrial Physics 65, 1329–1335, http://dx.doi.org/10.1016/j.jastp.2003.08.013.

Nakamura, T., Higashikawa, A., Tsuda, T., Matsushita, Y., 1999. Seasonal variations of gravity wave structures in OH airglow with a CCD imager at Shigaraki. Earth, Planets and Space 51, 897–906.

Nakamura, T., Aono, T., Tsuda, T., Admiranto, A.G., Achmad, E., Suranto, 2003. Mesospheric gravity waves over a tropical convective region observed by OH airglow imaging in Indonesia. Geophysical Research Letters 30, 1882–1885, http://dx.doi.org/10.1029/2003GL017619.

Nappo, C.J., 2002. An Introduction to Atmospheric Gravity Waves. Academic Press, California, USA.

Narayanan, V.L., Gurubaran, S., Emperumal, K., 2009a. A case study of a mesospheric bore event observed with an all-sky airglow imager at Tirunelveli (8.7°N). Journal of Geophysical Research 114, D08114, http://dx.doi.org/10.1029/2008JD010602.

Narayanan, V.L., Gurubaran, S., Emperumal, K., 2009b. Imaging observations of upper mesospheric nightglow emissions from Tirunelveli (8.7°N). Indian Journal of Radio and Space Physics 38, 150–158.

Narayanan, V.L., Gurubaran, S., Emperumal, K., 2010. Airglow imaging observations of small-scale structures driven by convective instability in the upper mesosphere over Tirunelveli (8.7°N). Journal of Geophysical Research 115, D19119, http://dx.doi.org/10.1029/2009JD012937.

Narayanan, V.L., Taori, A., Patra, A.K., Emperumal, K., Gurubaran, S., 2012a. On the importance of wave-like structures in the occurrence of equatorial plasma bubbles: a case study. Journal of Geophysical Research 117, A01306, http://dx.doi.org/10.1029/2011JA017054.

Narayanan, V.L., Gurubaran, S., Emperumal, K.. 2012b. Nightglow imaging of different types of events, including a mesospheric bore observed on the night of February 15, 2007 from Tirunelveli (8.7°N). Journal of Atmospheric and Solar-Terrestrial Physics 78–79, 70–83, http://dx.doi.org/10.1016/j.jastp.2011.07.006.

Nielsen, K., Taylor, M.J., Hibbins, R.E., Jarvis, M.J., 2009. Climatology of short-period mesospheric gravity waves over Halley, Antarctica (76°S, 27°W). Journal of Atmospheric and Solar-Terrestrial Physics 71, 991–1000, http://dx.doi.org/10.1016/j.jastp.2009.04.005.

Pautet, P.-D., Taylor, M.J., Liu, A.Z., Swenson, G.R., 2005. Climatology of short-period gravity waves observed over northern Australia during the Darwin Area Wave Experiment (DAWEX) and their dominant source region. Journal of Geophysical Research 110, D03S90, http://dx.doi.org/10.1029/2004JD004954.

Pragati, R.S., Parihar, N., Ghodpage, R., Mukherjee, G.K., 2010. Characteristics of gravity waves in the upper mesosphere region observed by OH airglow imaging. Current Science 98, 392–397.

Rajaram, R., Gurubaran, S., 1998. Seasonal variabilities of low-latitude mesospheric winds. Annales Geophysicae 16, 197–204.

Suzuki, S., Shiokawa, K., Hosokawa, K., Nakamura, K., Hocking, W.K., 2009a. Statistical characteristics of polar cap mesospheric gravity waves observed by an all-sky airglow imager at Resolute Bay, Canada. Journal of Geophysical Research 114, A01311, http://dx.doi.org/10.1029/2008JA013652.

Suzuki, S., Shiokawa, K., Otsuka, Y., Ogawa, T., Wilkinson, P., 2004. Statistical characteristics of gravity waves observed by an all-sky imager at Darwin, Australia. Journal of Geophysical Research 109, D20S07, http://dx.doi.org/10.1029/2003JD004336.

Suzuki, S., Shiokawa, K., Liu, A.Z., Otsuka, Y., Ogawa, T., Nakamura, T., 2009b. Characteristics of equatorial gravity waves derived from mesospheric airglow imaging observations. Annales Geophysicae 27, 1625–1629.

Suzuki, S., Tsutsumi, M., Palo, S.E., Ebihara, Y., Taguchi, M., Ejiri, M., 2011. Short-period gravity waves and ripples in the south pole mesosphere. Journal of Geophysical Research 116, D19109, http://dx.doi.org/10.1029/2011JD015882.

Swenson, G.R., Mende, S.B., 1994. OH emission and gravity waves (including a breaking wave) in all-sky imagery from Bear lake, UT. Geophysical Research Letters 21, 2239–2242, http://dx.doi.org/10.1029/94GL02112.

Taylor, M.J., Pendleton Jr., W.R., Clark, S., Takahashi, H., Gobbi, D., Goldberg, R.A., 1997. Image measurements of short-period gravity waves at equatorial latitudes. Journal of Geophysical Research 102, 26283–26299, http://dx.doi.org/10.1029/96JD03515.

Vincent, R.A., 1987. Planetary and gravity waves in the mesosphere and lower thermosphere. Advances in Space Research 7, 163–169.

Walterscheid, R., Hecht, J., Vincent, R., Reid, I., Woithe, J., Hickey, M., 1999. Analysis and interpretation of airglow and radar observations of quasi-monochromatic gravity waves in the upper mesosphere and lower thermosphere over Adelaide, Australia (35°S, 138°E). Journal of Atmospheric and Solar-Terrestrial Physics 61, 461–478.